Critical Isotherms from Virial Series Using Asymptotically Consistent Approximants

Nathaniel S. Barlow
School of Mathematical Sciences, Rochester Institute of Technology, Rochester, NY 14623

Andrew J. Schultz and David A. Kofke
Dept. of Chemical and Biological Engineering, University at Buffalo, State University of New York, Buffalo, NY 14126

Steven J. Weinstein
Dept. of Chemical and Biomedical Engineering, Rochester Institute of Technology, Rochester, NY 14623

DOI 10.1002/aic.14531
Published online June 25, 2014 in Wiley Online Library (wileyonlinelibrary.com)

The low-density equation of state of a fluid along its critical isotherm is considered. An asymptotically consistent approximant is formed having the correct leading-order scaling behavior near the vapor-liquid critical point, while retaining the correct low-density behavior as expressed by the virial equation of state. The formulation is demonstrated for the Lennard–Jones fluid, and models for helium, water, and n-alkanes. The ability of the approximant to augment virial series predictions of critical properties is explored, both in conjunction with and in the absence of critical-property data obtained by other means. Given estimates of the critical point from molecular simulation or experiment, the approximant can refine the critical pressure or density by ensuring that the critical isotherm remains well-behaved from low density to the critical region. Alternatively, when applied in the absence of other data, the approximant remedies a consistent underestimation of the critical density when computed from the virial series alone. © 2014 American Institute of Chemical Engineers *AIChE J*, 60: 3336–3349, 2014
Keywords: virial equation of state, critical phenomena, crossover, approximant, Lennard-Jones

Introduction

The virial equation of state (VEOS) describes the dependence of pressure on density via a series expansion about the ideal-gas limit[1]

$$P=kT\sum_{j=1}^{J}B_j\rho^j,\quad B_1=1 \tag{1}$$

where P is the pressure, ρ is the number density, k is the Boltzmann constant, and T is the absolute temperature. From here on, we refer to the J-term virial series as VEOSJ. The virial coefficients B_j are functions only of T, and the jth coefficient is given in terms of integrals over positions of j molecules.[2] Each increment in the order of the virial coefficient introduces an integration over an additional six variables for description of the new molecule's relative position and orientation, plus any other variables required to describe internal degrees of freedom. Moreover, the number of integrals appearing for each coefficient increases rapidly with the order j of the coefficient. The Mayer sampling Monte Carlo approach is an effective way to compute these integrals, using importance sampling.[3] This approach was recently used to obtain the first eight virial coefficients for the Lennard–Jones model,[4,5] the first five coefficients for an *ab initio* model of helium-4[6] (unpublished B_5 coefficients for He-4 are obtained in the same manner as those in Shaul et al.[6]), the first five coefficients of the Gaussian-charge polarizable model (GCPM) for water,[7] and the first 4–6 coefficients of transferable potentials for phase equilibria (TraPPE) alkanes.[8]

It has been known for some time that the virial series is able to provide a good estimate for the critical temperature.[9–11] The virial series has also been shown to predict values for the critical pressure that are very close to simulation data and experiments.[4,8] The criteria for locating the critical point of a pure substance are

$$\left(\frac{\partial P}{\partial \rho}\right)_{T,N}=0;\quad \left(\frac{\partial^2 P}{\partial \rho^2}\right)_{T,N}=0;\quad \left(\frac{\partial^3 P}{\partial \rho^3}\right)_{T,N}\geq 0 \tag{2}$$

where N is the number of molecules.[12] The equalities in (2) are solved for the critical temperature T_c and the critical density ρ_c, and (1) is then used to calculate the critical pressure P_c. When solved using a sufficiently high-order virial series, these predictions for T_c and P_c are often close to simulation data and/or experiments, but those for ρ_c are consistently about 10% too low in such a comparison.[4,8]

Underestimation of the critical density by the virial series is connected to the nonclassical behavior of real fluids at the critical point, for which critical scaling laws assert that ρ_c is a branch-point singularity of the function $P(\rho)$ along the critical isotherm. In the context of critical phenomena, the molar

Correspondence concerning this article should be addressed to N. S. Barlow at barlow.nate@gmail.com.

© 2014 American Institute of Chemical Engineers

volume is the appropriate variable for expressing the equation of state when selecting P as the dependent variable. The density ρ is preferred, however, because it provides for a more symmetric behavior about the critical point.[13,14] In this case, the chemical potential μ is the appropriate choice for the dependent variable, so the equation of state is expressed as $\mu(\rho)$. However, the critical exponent and amplitude for the leading singular behavior of $\mu(\rho)$ is the same as for $P(\rho)$,[13,14] and given that the virial series is most familiar and useful in the latter form, we use this in our development. The leading-order scaling along the critical isotherm ($T = T_c$) is given by[14–16]

$$\frac{P}{P_c} \sim 1 - D_0 \left(1 - \frac{\rho}{\rho_c}\right) \left|1 - \frac{\rho}{\rho_c}\right|^{\delta - 1} \quad \text{as} \quad \rho \to \rho_c \tag{3}$$

where $D_0 > 0$ is a fluid-specific critical amplitude. The critical exponent δ is exactly 3 for classical fluids (e.g., one described by a cubic equation of state), but for real (nonclassical) fluids in the 3-D Ising universality class, $\delta = 4.789 \pm 0.002$,[17] and thus ρ_c is a branch point. Consequently, a virial series describing a nonclassical fluid cannot be expected to converge at or beyond ρ_c, and will converge poorly on approach to ρ_c. This behavior leads to the systematic underestimation of ρ_c when computed by the virial series. Note that for a classical fluid, δ is an integer and there is no singularity at ρ_c. Hence, a virial series describing a classical fluid is expected to converge up to and beyond ρ_c, and a calculation of ρ_c from the virial series will be consistent with the value obtained directly from the model defining the classical fluid.

In this work, we use approximants to analytically continue the virial series such that it captures the behavior described above, allowing us to construct isotherms that have both the correct low-density and critical asymptotic behaviors. In the context of the virial series, an approximant is a function whose Taylor expansion about $\rho = 0$ matches VEOSJ to order ρ^J in (1). A review of various approximant types is given in Chisholm.[18] If the virial series has an inherent radius of convergence (here, certainly no larger than ρ_c for real fluids at T_c), an approximant can sometimes be used to analytically continue the series beyond this radius. There are, however, an infinite number of analytic continuations that correspond to a truncated series, through an infinite variety of approximants. Therefore, it is essential to have, in supplement with the virial series, additional information about the $P(\rho)$ behavior for the fluid isotherm being described. This allows one to choose an appropriate class of approximants that analytically continue the virial series.

For example, it has been a frequent practice to choose approximants containing a singularity when forming an analytic continuation of the virial series for hard-sphere fluids, as it is believed that either a physical or nonphysical density-singularity could set the series' radius of convergence (see Maestre et al.[19] and references therein). These approximants are used to either predict or enforce the singularity.[20–23] In this work, we use approximants in both ways. In addition, the approximants constructed here fall under the class of asymptotically consistent approximants, in that the asymptotic behavior of the approximant is consistent with the asymptotic behavior of the fluid toward the desired region of continuation. The seminal example of this was given by Baker and Gammel,[24] who suggested that such approximants can be used to obtain optimal convergence acceleration. This is indeed the case for very soft soft-sphere fluids, where asymptotically consistent approximants have recently been applied to analytically continue the virial series into the large-ρ regime.[25] In the present work, the desired region of continuation is instead in the vicinity of the critical point.

Use of approximants to characterize critical phenomena is well-established in the context of lattice models.[17,26–28] An early example is the prediction of T_c using high-temperature expansions along a critical isochore[29] where ρ_c is exactly known. Given the large number of terms available for these series[30,31] and the rapid approach toward critical scaling, approximants not only predict T_c to a high degree of accuracy for lattice models, but also provide an accurate value for the relevant critical exponent (see Thompson[32] and references therein). The approach is not as straightforward when applied to the virial series of a real fluid along the critical isotherm, as T_c is not exactly known. Additionally, there are typically not enough terms to see a limiting behavior using standard series analysis techniques (e.g., ratio-method, Padé approximants, and so forth[28]). Instead, critical properties of real fluids from the virial series are typically obtained through the application of (2) toward (1) such that the thermodynamic definition of a critical point is satisfied at the desired order J. With the advancement of computational architecture (e.g., graphics processors[5]) and algorithms[3,33] that allow one to compute higher-order virial coefficients for off-lattice systems, the ability of density series to predict and characterize the critical point is worth serious consideration, beyond the simple application of (2). Bondarev[34] recently attempted this, separating the pressure into an analytic contribution using low-order virial coefficients, and a nominally singular contribution using the remainder of the series. The behavior of his treatment at the critical point is consistent with (3) but requires $\delta = 4$, and accordingly yields an inaccurate critical density—10% too high, in comparison to molecular simulation results.

Thus the present work is driven by an interest in using the virial coefficients to provide reliable predictions of the critical properties. An appropriate starting point toward this goal is consideration of behavior along the critical isotherm, and consequently that is our focus here. Formulation of a temperature-dependent global equation of state, fully consistent with the low-density virial series as well as all universal singular behaviors, is a larger problem of considerable interest, but is not attempted here.

The article is organized as follows. In the first few sections of the article, the critical temperature, pressure, and density are taken as given. In this context, an approximant is proposed that links the low-density behavior given by the virial series with the nonclassical critical scaling behavior along the critical isotherm. The approximant is then used to describe both classical and nonclassical fluid models. A closed-form description is provided for the vapor side of the critical isotherm for the Lennard–Jones fluid, He-4, and GCPM water. In the sections that follow this initial treatment, the approximant is applied toward evaluation of the critical properties, specifically the critical density (for Lennard–Jones), critical pressure (for model alkanes), and a critical amplitude (for several fluids). A comparison is then made between the approximant and an established comprehensive crossover model. In the final section of the article, overall conclusions and suggestions for further development are provided.

Critical Isotherms from Approximants

In this section, critical isotherms are constructed using given values of the critical density ρ_c, critical pressure P_c,

critical temperature T_c, and critical exponent δ. These values can come from either experiments, molecular simulation, direct virial-series predictions, or approximant predictions such as those given in a later section, "Critical properties from approximants."

An approximant that matches the critical scaling law (3) for the region $\rho \leq \rho_c$ is given by

$$P = P_c - A(\rho)\left(1 - \frac{\rho}{\rho_c}\right)^{\delta} \tag{4a}$$

where $\delta > 0$. P_c represents the nonsingular "background" contribution; in general, this is a function of temperature,[14,35] but here it is just a constant, as we are focused on the critical isotherm. The function $A(\rho)$ used here is a polynomial, which can be thought of as the Taylor expansion of $[P_c - P(\rho)](1-\rho/\rho_c)^{-\delta}$ about $\rho = 0$, which is truncated to form the approximant. If δ is a noninteger, as is the case for real fluids, (4a) enforces that the closest singularity to $\rho = 0$ (in the complex ρ-plane) is ρ_c. In principle, the scaling law represented in (4a) should be written in terms of generalized scaling fields, which in turn are formed as functions of the thermodynamic fields (temperature, chemical potential, and pressure).[16,40–42] Moreover, even with properly formulated scaling fields, there exists correction-to-scaling terms that describe higher-order effects.[43,44] Failure to include these introduces additional, weaker singularities at $\rho = \rho_c$ (i.e., "confluent singularities"[37]) that must be absorbed into $A(\rho)$. If critical exponents are noninteger rational numbers, then the corrections-to-scaling series along the critical isotherm[36,37] suggests that ρ_c has the character of a transcendental (essential) branch point.[38] If at least one critical exponent (such as δ) is found to be irrational, ρ_c would then have the character of a logarithmic branch point.[39] Without incorporating all confluent singularities, we are prevented from constructing an approximant to describe the region $\rho > \rho_c$. We must also recognize that any practical implementation of (4a) will necessarily be done with inexact values of δ and ρ_c. Thus, in principle and in practice, $A(\rho)$ is itself singular, but more weakly so than $P(\rho)$, and consequently, it may be expected that its expression as a density series will have better convergence properties than exhibited by the virial series alone.

Apart from its incomplete handling of residual confluent singularities at the critical point, implicit in our approximant formulation is the assumption that no singularity exists in the region $|\rho| < \rho_c$ along the critical isotherm. Fluids with a vapor-liquid transition have long been modeled under the assumption that no singularities exist in the one-phase region.[16,44,45] However, this can be proved only on a case-by-case basis and in the limit of an infinite-term virial series (i.e., an exact equation of state). Here, convergence of the approximant (as additional terms are included) is used as a metric for determining its efficacy.

The J-term expansion of approximant (4a) about $\rho = 0$ matches the J-term virial series (1) exactly when $A(\rho)$ is given by

$$\begin{aligned} A(\rho) &= P_c + \sum_{j=1}^{J} a_j \rho^j, \\ a_j &= \frac{P_c\ \Gamma(\delta+j)}{j!\ \rho_c^j\ \Gamma(\delta)} - \frac{kT_c}{\Gamma(\delta)} \sum_{n=0}^{j-1} \frac{B_{j-n}\ \Gamma(\delta+n)}{\rho_c^n\ \Gamma(n+1)}. \end{aligned} \tag{4b}$$

Formulas (4a) and (4b) allow one to construct critical isotherms for any fluid, given input values of ρ_c, P_c, T_c, and δ. For example, the $J = 1$ critical approximant given in Appendix A is valid for any fluid, since $B_1 = 1$ for any fluid (ideal gas limit as $\rho \to 0$). Each additional virial coefficient allows one to generate an additional a_j coefficient in (4b). From here on, we refer to the approximant constructed from VEOSJ as AJ, where J is the number of available virial coefficients. These newly generated critical isotherms are guaranteed to match the low-density behavior provided by the virial series as well as the nonclassical scaling behavior near the critical point. In this sense, they are multipoint approximants.

For $\rho < \rho_c$, (3) becomes $P_c - P \sim D_0 P_c/\rho_c\ (\rho_c - \rho)^{\delta}$ in the immediate vicinity of the critical point. If one has access to the location of the critical point as well as an accurate description of $P(\rho)$ along the critical isotherm, the value of the critical exponent can be evaluated as the limit

$$\delta = \lim_{\rho \to \rho_c} \delta_{\text{eff}}, \tag{5a}$$

where δ_{eff} is an effective exponent

$$\delta_{\text{eff}} = \left[\frac{\partial\ \ln(P_c - P)}{\partial\ \ln(\rho_c - \rho)}\right]_{T_c} = \left[\frac{\rho_c - \rho}{P_c - P}\left(\frac{\partial P}{\partial \rho}\right)\right]_{T_c} \tag{5b}$$

This quantity is useful when examining the approach of approximants and the virial series to critical scaling behavior, as shall be demonstrated in the next few sections.

Application to a classical fluid

Let us first give a simple example of applying approximant (4). The van der Waals equation of state is written in nondimensional form as

$$P^\star = \frac{\rho^\star T^\star}{1 - \rho^\star} - \rho^{\star 2} \tag{6}$$

where $\rho^\star = C_1\rho$, $P^\star = C_1^2 P/C_2$, $T^\star = kTC_1/C_2$, and the parameters C_1 and C_2 describe the intermolecular attraction and repulsion, respectively. The critical properties of (6) are $\rho_c^\star = 1/3, P_c^\star = 1/27$, and $T_c^\star = 8/27$, which is easily verified through application of definitions (2). The critical exponent formula (5) applied to (6) leads to $\delta = 3$, as expected for a classical fluid. One advantage of testing our approximant on a model such as this is that the equation of state (6) is known exactly. Hence we can generate an infinite number of exact virial coefficients; they are given by the coefficients of the expansion of $P^\star/(\rho^\star T^\star)$ about $\rho^\star = 0$, which are simply $B_2 = (1 - 1/T^\star)$ and $B_{j>2} = 1$.

The van der Waals model is different from nonclassical models in that there is no branch-point singularity at the critical point. The only finite singularity of (6) is the pole $\rho = 3\rho_c$ (i.e., $\rho^\star = 1$), so we are guaranteed convergence of the virial series of (6) in the region $\rho < 3\rho_c$. Approximant (4) accelerates this convergence by enforcing the correct asymptotic critical behavior, as shown in Figure 1a. On the scale of the figure, A1, A4, and A7 are indistinguishable from each other in the region $\rho < \rho_c$, which is not the case for the virial series. Note that (on this scale) the 1-term approximant A1, which uses the ideal-gas law (VEOS1) as an input, performs as well as VEOS7 in the region $\rho < \rho_c$. We can also examine the behavior for $\rho > \rho_c$ since δ is an odd integer, which means that the approximant captures the scaling behavior approached from both sides of ρ_c. As shown in Figure 1a, both the approximant and virial series converge to the exact equation of state (6) (•) up to and

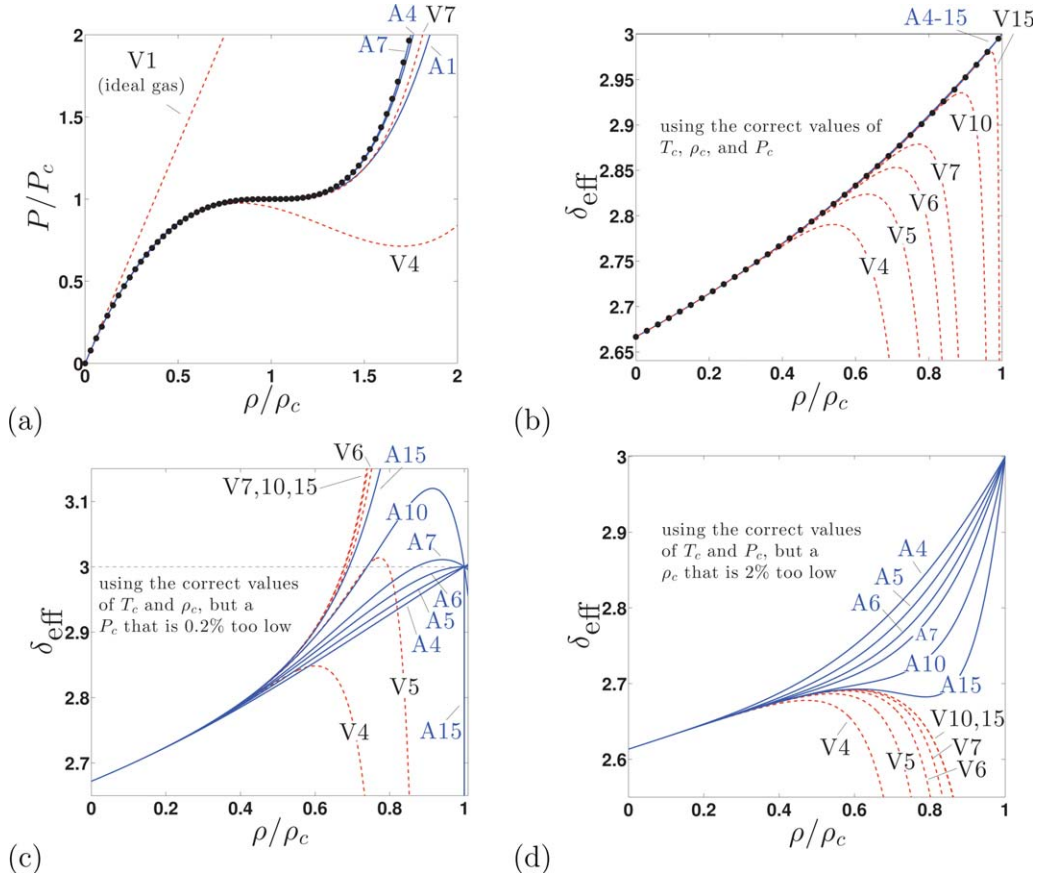

Figure 1. Critical isotherm of the van der Waals model.

(a) van der Waals equation 6 (•), virial series (- -, VEOS*J* abbreviated as V*J*), approximant(—, A*J*) using ρ_c, P_c, and T_c as inputs; and (b–d) approach to critical scaling along the critical isotherm, given by (5b) using critical properties as specified in the plot. [Color figure can be viewed in the online issue, which is available at wileyonlinelibrary.com.]

beyond ρ_c; it is evident, however, that the approximant tracks the exact behavior more closely as ρ gets larger, does so using fewer virial coefficients as input, and apparently converges more quickly than the virial series for $\rho > \rho_c$.

Figure 1b shows the approach to critical scaling, where (5b) is applied to the virial series and approximant at various orders. The value of δ approximated by the virial series becomes closer to $\delta = 3$ as more terms are included, in accordance with (5a). The nonuniform convergence of these curves is a result of a singularity in (5b) occurring where the pressure described by the virial series (at each order) becomes equal to P_c. The approach to the correct scaling behavior in Figure 1b indicates that we are using virial series along the correct critical isotherm, as well as using the correct values of ρ_c and P_c as inputs to (5b). Indeed, it is instructive to examine how Figure 1b differs if implemented using inaccurate critical parameters. This is illustrated in parts (c) and (d) of the figure. Figure 1c is constructed using P_c that is 0.2% too low, and Figure 1d shows the effect of making ρ_c 2% too low. Poor convergence is observed for both the original virial series, and the approximant. In some cases, the curves become discontinuous (e.g., A15 in Figure 1c). Similar effects (not shown here) result from inaccurate T_c (manifested in inaccurate virial coefficients), and from various combinations of critical-parameter inaccuracies.

A comparison of Figures 1a and 1b indicates that the tracking of $\delta_{\rm eff}$ at increasing orders of the virial series is a more sensitive measure of convergence than viewing P versus ρ, at least in the critical region where the correct degree of flatness is asymptotically approached. This method for viewing the approach to critical scaling becomes increasingly useful in the following section, where fluids are considered that have a limited number of virial coefficients available.

Application to molecular-model fluids

In this section, we use the nonclassical value of $\delta = 4.789$ and construct critical isotherms for the Lennard–Jones fluid,[2] an *ab initio* model of He-4,[46,47] and GCPM water.[48] The properties in Table 1 are used as inputs to (4) to generate the isotherms in the following figures. Virial coefficients evaluated at T_c are also given in the table, computed using an interpolation scheme[52] applied to the available virial coefficients for the Lennard–Jones fluid,[5] He-4[6], and GCPM water.[7] Since we are no longer working with a simple equation-of-state model fluid with an exact δ, and we are also neglecting nonleading scaling terms, $A(\rho)$ contains residual confluent singularities at $\rho = \rho_c$ remaining from $P(\rho)$, and the approximant (4) is applicable only for $\rho < \rho_c$; accordingly, we do not present results for densities larger than ρ_c.

Critical isotherms for the Lennard–Jones fluid, He-4, and GCPM water are shown in Figure 2. All curves in the figure are taken at the T_c values given in Table 1. The approximants A*J* in Figure 2 are constructed from (4) using the P_c and ρ_c values also given in Table 1. In the figure,

Table 1. Virial Coefficients and Critical Properties of Several Fluids Studied in this Work

	Lennard–Jones	He-4	GCPM water
T_c	1.313(1)	5.197(3) K	642.21 K
$(B_2)_{T_c}$	−3.25641527	−61.154(4) (cm^3/mol)	−0.07426(2) L/mol
$(B_3)_{T_c}$	2.571108893	960.4(11) (cm^6/mol^2)	1.56(5) × 10^{-4} $(L/mol)^2$
$(B_4)_{T_c}$	2.8607(4)	1.76(4) × 10^4 ($cm^9/mol^{3)}$	2.18(5) × 10^{-4} $(L/mol)^3$
$(B_5)_{T_c}$	0.615(9)	3(17) × 10^4 (cm^{12}/mol^4)	7(1) × 10^{-6} $(L/mol)^4$
$(B_6)_{T_c}$	−5.87(7)		
$(B_7)_{T_c}$	4.0(14)		
ρ_c	0.317(1)	0.01738(3) (mol/cm^3)	18.562 (mol/L)
P_c	0.1279(6)	227.2(6) (kPa)	24560 (kPa)

Lennard–Jones critical properties[49,50] and virial coefficients are given in reduced Lennard–Jones units. For He-4 and GCPM water, critical properties are taken respectively from Kukarin et al.[51] and Paricaud et al.[48] Virial coefficients for Lennard–Jones and He-4 at T_c are obtained using an interpolation scheme[52] applied to the coefficients[4–6] (unpublished B_5 coefficients for He-4 are obtained in the same manner as those in Shaul et al.[6]), except B_2 and B_3 for Lennard–Jones, which are given exactly. Virial coefficients for GCPM water are taken from Benjamin et al.[7] Numbers in parentheses specify the uncertainty on the last digit, either taken from the above references (for simulation and experiment values) or given as the 68% uncertainty (for virial coefficients).

approximants and virial series are compared against simulation data for the Lennard–Jones model, data from experiments for He-4, and the Wertheim equation of state (WEOS) for GCPM water. Note that the low-density series given by the WEOS is truncated at various orders (just as the truncated virial series, it is not exact) and is shown because of its superior convergence over the virial series.[57]

In all plots of Figure 2, $A1$ (the approximant solely using $B_1 = 1$) captures both the low-density behavior and higher-density critical behavior, by construction. Although the correct shape is captured by $A1$ in the intermediate region $0 \leq \rho \leq \rho_c$, the description can be improved by including additional virial coefficients in the approximant, as seen in Figure 2. When comparing curves in the figure, note that AJ includes a polynomial [the $A(\rho)$ portion of (4)] that is the same order in ρ as VEOSJ. For all fluids, the approximant accelerates the convergence of the virial series.

Figure 2 provides some insight into why the virial series is successful at predicting accurate values of T_c and P_c, even while ρ_c is too low. Recalling that the expected radius of convergence of the virial series is ρ_c, it is not possible to accurately predict ρ_c from the virial series using (2), as the series will never converge at ρ_c. However, the pressure described by the true equation of state becomes quite flat for some density $\rho < \rho_c$, wherein $P/P_c \approx 1$. In this region, convergence of the VEOS is possible (e.g., Lennard–Jones, Figure 2a), and virial series predictions of the critical pressure and temperature can be nearly correct even though the

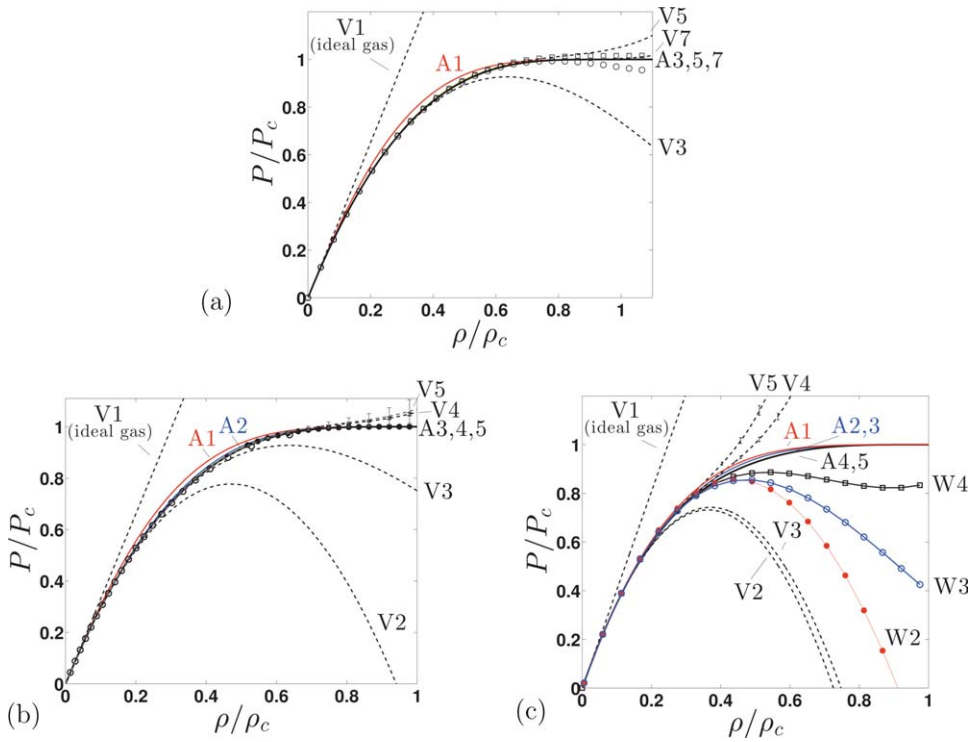

Figure 2. Critical isotherms prescribed by the virial series (Eq. 1, - -, VEOSJ abbreviated as VJ), and by approximants (Eq. 4, —, AJ) using ρ_c, P_c, T_c, and virial coefficients as inputs (Table 1).

(a) Lennard–Jones fluid: additional equations of state taken from Kolafa and Nezbeda[53] (○) and Johnson et al.[54] (□), which were constructed using molecular simulation data; (b) He-4: additional equations of state taken from the NIST WebBook[55] (○) and Bezverkhy et al.[56] (●), constructed using data from experiments; and (c) GCPM water: WEOSJ taken from Kim et al.[57] (curves with symbols, abbreviated as WJ). Error-bars specify the 68% uncertainty, propagated from uncertainty in the virial coefficients. [Color figure can be viewed in the online issue, which is available at wileyonlinelibrary.com.]

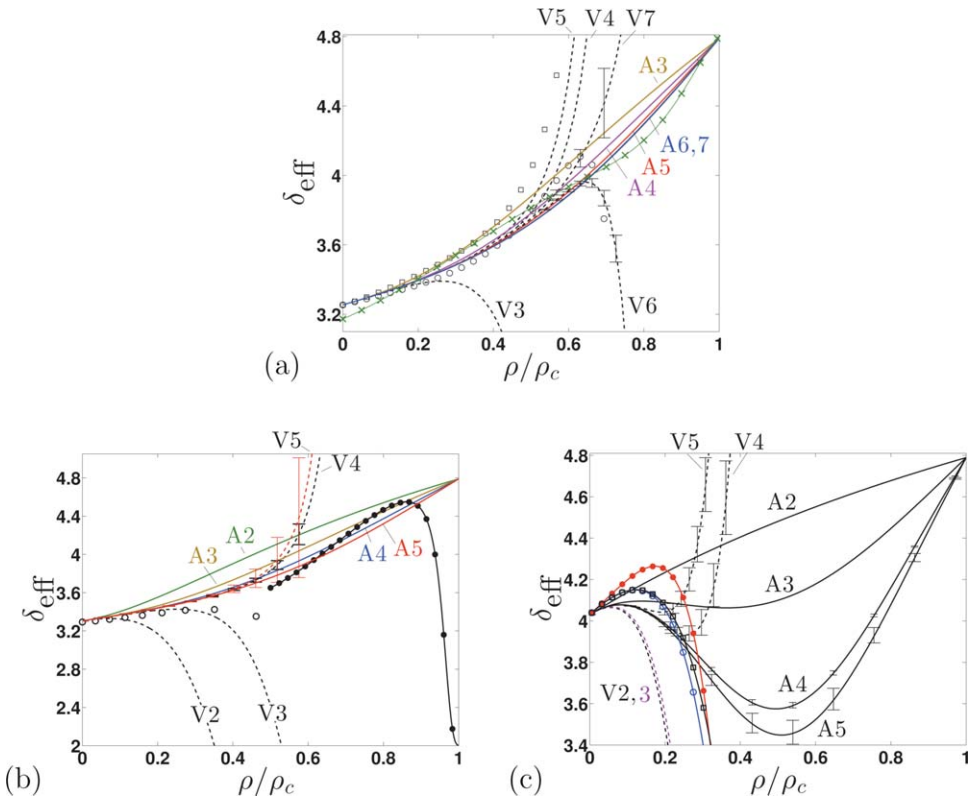

Figure 3. Approach to scaling along critical isotherms prescribed by (5b) using $P(\rho)$ from the virial series (Eq. 1, - -, VEOS*J* abbreviated as V*J*), and approximants (Eq. 4, —, A*J*) with ρ_c, P_c, T_c, and virial coefficients taken as inputs (Table 1).

(a) Lennard–Jones fluid: additional equations of state taken from Kolafa and Nezbeda[53] (○) and Johnson et al.[54] (□), constructed using molecular simulation data. A crossover model (see Appendix C) is also shown (–×–); (b) He-4: additional equations of state taken from the NIST WebBook[55] (○) and Bezverkhy et al.[56] (–•–), constructed using data from experiments; and (c) GCPM water: WEOS curves taken from Kim et al.[57] (symbols, see Figure 2c). Error-bars specify the 68% uncertainty, propagated from uncertainty in the virial coefficients. For all curves (except the crossover model), ρ_c in the *x*-axis is the value given in Table 1. [Color figure can be viewed in the online issue, which is available at wileyonlinelibrary.com.]

critical density is inaccurate. This effect is explored for a model problem in Appendix B. For the critical isotherms of GCPM water shown in Figure 2c, we do not have enough terms to establish convergence of the virial series at densities that reach the limiting $P/P_c \approx 1$ "flat" region—there are not yet enough virial coefficients available. We return to a discussion of the prediction of critical properties from virial series in a later section of this article, "Critical properties from approximants."

In Figure 3, convergence of the virial series and approximants is shown using Eq. (5b), which allows us to examine the approach toward critical scaling. Note that the $\rho = 0$ intercept on plots such as those in Figure 3 is always (for any fluid) $\rho_c kT_c/P_c \equiv 1/Z_c$, as can be verified in (5). The quantity $|1/Z_c - \delta|$ is a measure of the distance between critical δ-scaling behavior and low-density behavior, provided that the approach to scaling is monotonic. For Lennard–Jones (Figure 3a) and He-4 (Figure 3b), a continuous monotonic approach toward critical scaling is observed from $\delta_{\rm eff} = 1/Z_c$ at $\rho = 0$, to δ at $\rho = \rho_c$. Additionally, for these two models, the virial series converges along the approximant curves, and one might expect that these march further along with additional virial coefficients, as we saw for the van der Waals model (Figure 1b). Figure 3c highlights the relatively poor convergence of sequences of approximants, virial series, and WEOS*J* for GCPM water, as additional terms are included. As seen in the figure, each of these sequences converges only for densities less than 10% of ρ_c. Note also that the approach to critical scaling for GCPM water approximants is not monotonic, in contrast with that of Lennard–Jones and He-4. For all cases in which we have observed convergent approximants, a well-behaved (continuous and monotonic) approach to critical scaling is evident (Figures 1b and 3a, b). We speculate that this character is a necessary feature of successful critical approximants.

The semiempirical equation of state for helium-4, given in Bezverkhy et al.,[56] is used to represent data from experiments in Figures 2b and 3b (shown as –•–). In this model, a classical part and nonclassical part are combined through a Gaussian crossover function. While the nonclassical part alone attains the correct limit of $\delta_{\rm eff} \to \delta$ as $\rho \to \rho_c$ (not shown in figure), the Gaussian crossover function overrides this effect and causes $\delta_{\rm eff} \to 2$ at ρ_c, as seen in Figure 3b (which means that the critical criteria, Eq. 2, are not satisfied). We see, then, that $\delta_{\rm eff}$ is a sensitive measure of the shape of the isotherm, and can uncover anomalies even when the description of $P(\rho)$ is in sensible agreement with simulation or experiment.[56] In the section Comparison with a Crossover Model, a different type of crossover model is explored, one that reaches the correct asymptotic limit as $\rho \to \rho_c$ (shown in Figure 3a, –×–).

An additional feature of the approximant is its suppression of uncertainty propagated from the virial coefficients, as observed in Figures 2 and 3. Consequently, the approximant provides not only a more accurate but also a more precise description of the critical isotherm than the virial series. This is shown clearly in the two highest-order series of each plot in Figure 3. For He-4 and Lennard–Jones, the approximant matches the (already precise) virial series at low density. At $\rho \approx \rho_c/2$, the virial series begins to accrue significant error (i.e., error-bars are visible on the scale of the plot); the approximant, however, remains precise over the entire range $0 < \rho < \rho_c$ (i.e., error-bars are smaller than line-width). This is true to a lesser extent for GCPM water, as seen in Figures 2c and 3c.

The performance for GCPM water notwithstanding, the results given here encourage the development of approximant-based tools that can be used to predict critical properties, so we turn to this topic in the next section.

Critical Properties from Approximants

As mentioned in the Introduction, approximants have been successfully applied in the prediction of the critical temperature and exponent of lattice systems, given a high-temperature series along the path of the critical isochore.[26] In much the same way, we may relax one degree of freedom in (4) by reducing the order of the polynomial (4b) and predict the critical density or pressure, given the low-density (virial) series along the critical isotherm of a real fluid. This is equivalent to setting $a_J = 0$ in (4b), leading to

$$P_c - \frac{kT_c J!}{\Gamma(\delta+J)} \sum_{j=1}^{J} \frac{\Gamma(\delta+J-j)}{\Gamma(J-j+1)} B_j \rho_c^j = 0. \tag{7}$$

Given a J-term virial series evaluated at a known T_c, (7) can be used to either (1) solve for P_c, given ρ_c or (2) solve for the J roots of ρ_c, given P_c. In either case, the approximant describing the isotherm is then given by (4) with $A(\rho)$ now having $J-1$ coefficients obtained using (4b). When predicting ρ_c using (7), J possible approximants are then obtained for each order J, as prescribed by the J possible ρ_c roots. For our prediction of critical density at each order J, we choose the ρ_c root which leads to the most rapidly converging approximants as additional terms are included in the series.

We shall now give two examples of the application of (7) to predict critical properties. In the first example, we predict ρ_c for the Lennard–Jones fluid, given P_c and T_c from both the virial series and from molecular simulation. Then, we predict P_c for model alkanes, given ρ_c and T_c from molecular simulation.

Predicting ρ_c, given P_c and T_c

If we accept the hypothesis that ρ_c is the radius of convergence of the virial series describing the critical isotherm, the prediction for ρ_c using the virial series will always be too low, as seen for Lennard–Jones,[4] model alkanes,[8] and demonstrated for a model problem in Appendix B. However, as additional virial coefficients are included, the critical isotherm predicted by the virial series is expected to become nearly flat prior to reaching the critical point (cf. Figures 2a, b), providing accurate estimates for P_c and T_c despite the inaccuracy in ρ_c. These quantities can then be used as inputs to (7) to predict an accurate branch point ρ_c, which is consistent with the approximant. In what follows, this is demonstrated for the Lennard–Jones fluid.

In the first 4 columns of Table 2, predictions of critical properties are given for the Lennard–Jones fluid using recently obtained virial coefficients.[5] These properties are determined by finding values that satisfy definitions (2) for each order J of the virial series (1). It is clear from the table that additional coefficients are needed to establish convergence. Also, the value of $\rho_{c,\mathrm{VEOS7}}$ is roughly 10% lower than the value from molecular simulation $\rho_{c,\mathrm{sim}}$ (Table 2, bottom row). As higher-order virial coefficients become available for this and other model fluids, we anticipate that the prediction of $\rho_{c,\mathrm{VEOS}J}$ will always be inaccurate, due to convergence limitations discussed above (again, see Appendix B). To remedy this, we use (7) to obtain a corrected value of the critical density $\rho_{c,\mathrm{A}J}$ (Table 2, rightmost column). We choose the smallest real positive ρ_c root of the J possible roots of (7), as it leads to the most rapidly converging approximant when used in (4). When comparing values in the table and subsequent figures, note that the subscript AJ refers to an approximant that includes a polynomial that is one order less in ρ than VEOSJ, as we have sacrificed a coefficient of $A(\rho)$ in (4) to predict ρ_c, resulting in (7).

The deviation between $\rho_{c,\mathrm{A}J}$ and $\rho_{c,\mathrm{sim}}$ is shown in Figure 4, plotted versus the inverse of the series order $1/J$, allowing us to envision possible extrapolations to the infinite series $(1/J = 0)$ limit. In Figure 4a, predictions of ρ_c, T_c, and P_c vary at each order J. Although the predictions $\rho_{c,\mathrm{A}J}$ using (7) (•) do not converge any faster than predictions $\rho_{c,\mathrm{VEOS}J}$ from the virial series (□), they approach a value closer to $\rho_{c,\mathrm{sim}}$ as J increases.

The sensitivity of ρ_c to given P_c and T_c as inputs to the approximant (7) is illustrated in Figure 4b, where the ρ_c prediction curves are evaluated at indicated fixed values of T_c and P_c (given in Table 2) obtained from a truncation of the virial series; the truncation order is indicated for each curve in the subscript of T_c. As shown in the figure, prediction curves evaluated at temperatures close to $T_{c,\mathrm{sim}}$ follow a linear trend toward $J = \infty$, all extrapolating to a value lower than $\rho_{c,\mathrm{sim}}$. However, as demonstrated in Figure 4a, the predictions of ρ_c, T_c, and P_c change at each order J, and so the trends in Figure 4b are not necessarily indicative of the ultimate prediction of ρ_c; this would be obtained from Figure 4a. Figures 4a, b together suggest that convergence of ρ_c predictions is likely to occur, but it is clear that additional virial coefficients are required to deduce the limiting behavior.

Predicting P_c, given ρ_c and T_c

As shown in a previous section (Critical Isotherms From Approximants), the approach of the virial series and the approximant toward critical scaling can be examined on a δ_{eff} versus ρ plot. In constructing such a plot, a well-behaved approach of the effective exponent δ_{eff} toward the actual critical exponent δ relies on accurate values of T_c, P_c, and ρ_c as inputs to (5b). The good convergence shown in Figures 1b and 3a, b for the van der Waals model, Lennard–Jones fluid, and He-4, respectively, indicate that the approximants are based on accurate values of the critical parameters. In contrast, Figures 1c, d show how poor convergence of the approximant can result from inaccuracy in the critical properties on which it is based. Accordingly, if the available literature values of the critical properties do not lead to

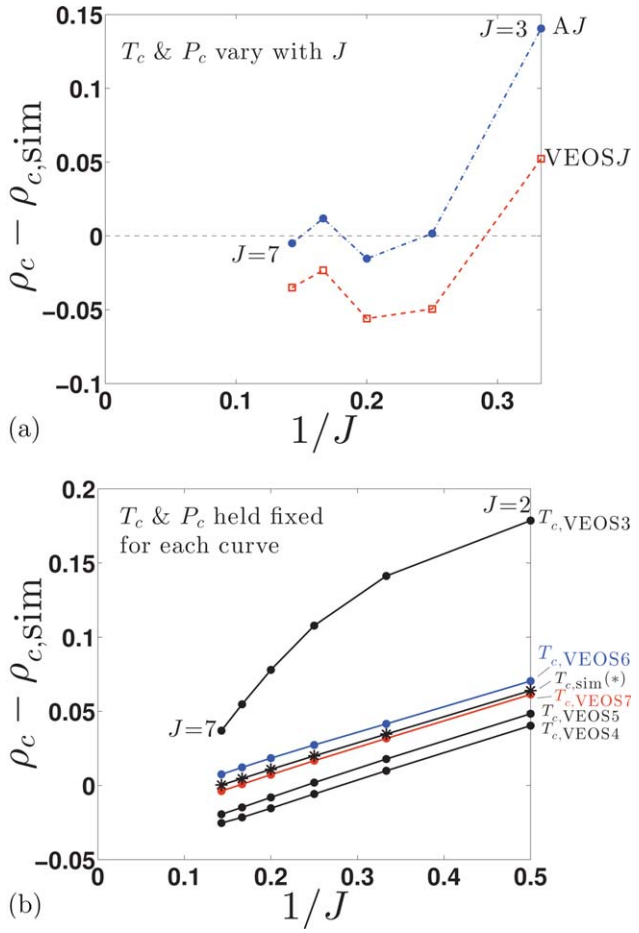

Figure 4. Deviation between ρ_c from the approximant [using (7)] and $\rho_{c,\mathrm{sim}}$,[49,50] plotted versus order 1/J, where J is the number of virial coefficients used in forming the approximant.

(a) predictions from VEOSJ (□) and AJ (•) using T_c and P_c values that vary along the 1/J-axis; these correspond with the two right-most columns of Table 2. (b) each curve represents a sequence of approximants (A2 through A7) evaluated for a single prediction of T_c and P_c from either the virial series or simulation. [Color figure can be viewed in the online issue, which is available at wileyonlinelibrary.com.]

approximants and virial series that approach the correct critical scaling in a well-behaved way, one may consider adjusting the values within their error-bars until such scaling behavior is obtained.

We attempted this procedure for GCPM water to "correct" Figure 3c, but we were unable to find critical values that yielded a substantial improvement. We conclude that for this model, we simply do not have enough virial coefficients for a density series to reach the critical region, or the pressure plateau, where enforcement of the asymptotic behavior can aid the series convergence. However, an application for certain model alkanes has been fruitful, so we turn to them to demonstrate the approach.

For TraPPE alkanes, the uncertainties in the available molecular simulation estimates of critical pressure are larger than that of critical density and temperature.[58] For this reason, we use the nominal simulation values of ρ_c and T_c as an input to the approximant (4) and adjust P_c within its error-bars until a well-behaved (presumed monotonic) approach to scaling is obtained. Fortunately, one can use an approximant to directly provide the best value for a well-behaved approach to critical scaling, if one exists. In this section, we use (7) to predict P_c, given simulation values for ρ_c and T_c. This critical pressure is then used as an input to (4) (AJ) where approximant coefficients are generated using (4b).

Let us begin by applying this technique to TraPPE ethane.[58] The critical properties of TraPPE ethane from molecular simulation are $T_c = 304(2)$ K, $P_c = 5.1(4)$ MPa, and $\rho_c = 0.206(3)$ g/ml.[58] Using these values and the virial coefficients (Table 3) as an input to (4), the approximant is constructed. As shown in Figure 5a, the approach to critical scaling is discontinuous, as evidenced in particular by the curves for A5 and A6. This behavior is suggestive of that seen for the van der Waals model with incorrect critical parameters, shown in Figures 1c, d. To correct it, we use the virial coefficients and the values of ρ_c and T_c from simulation to generate estimates of P_c from (7); for TraPPE ethane, these are (using VEOS2 to 6): 4.6783(2), 5.0453(3), 5.1902(5), 5.2530(7), and 5.281(1) MPa. Numbers in parentheses specify the 68% uncertainty on the last digit, propagated from uncertainty in the virial coefficients. Now, using the estimate from VEOS6 ($P_{c,\mathrm{A6}} = 5.281$ MPa) as an input to (4), the approximant is constructed for each order J. Note that the approximant A6 includes a polynomial that is one order less in ρ than VEOS6, as we have sacrificed a coefficient of $A(\rho)$ in (4) to predict P_c. However, all lower-order approximants A($J < 6$) that use $P_{c,\mathrm{A6}}$ include a polynomial, which is the same order as VEOSJ. As shown in Figure 5b, the approach to scaling is now continuous using the value of P_c from the approximant, which is within the error-bars of the simulation value, $P_c = 5.1(4)$ MPa. We repeat this process for TraPPE propane, butane, pentane, octane, and dodecane. The simulation critical point estimates and relevant virial coefficients used to compute $P_{c,\mathrm{A}J}$ for these alkanes

Table 2. Critical Properties of the Lennard–Jones Fluid as Predicted by VEOSJ

J	$T_{c,\mathrm{VEOS}J}$	$P_{c,\mathrm{VEOS}J}$	$\rho_{c,\mathrm{VEOS}J}$	$\rho_{c,\mathrm{A}J}$
3	1.445277391	0.177913682	0.369269712	0.45752475
4	1.299174(13)	0.122301(19)	0.267471(7)	0.3185970(5)
5	1.29059(9)	0.11934(3)	0.26098(7)	0.301605(1)
6	1.3186(4)	0.13020(17)	0.2936(6)	0.32884(2)
7	1.311(2)	0.127(1)	0.281(3)	0.31199(5)
sim[49,50]	1.313(1)	0.1279(6)	0.317(1)	0.31668(5)[a]

Values are given in Lennard-Jones units. Virial coefficients are from Schultz et al.[5] $\rho_{c,\mathrm{A}J}$ is the corrected critical density given by the smallest positive root of (7), which takes the following as inputs: $\delta = 4.789$; P_c, ρ_c, and T_c as predicted by the virial series at each order J (given above); and the corresponding virial coefficients (taken from an interpolation). Numbers in parentheses specify the 68% uncertainty on the last digit, propagated from uncertainty in the virial coefficients (with the exception of the simulation values).

[a]Predicted using (7) with $P_{c,\mathrm{sim}}$, $T_{c,\mathrm{sim}}$, and the first seven virial coefficients taken at $T_{c,\mathrm{sim}}$ (from an interpolation) as inputs.

Table 3. Critical Properties and Virial Coefficients of TraPPE Alkanes

	Ethane	Propane	Butane	Pentane	Octane	Dodecane
$T_{c,sim}$ (K)	304(2)	368(2)	423(4)	470(4)	570(2)	667(5)
$(B_2)_{T_c}$ (L/mol)	−0.15239(1)	−0.21155(4)	−0.27404(3)	−0.34037(8)	−0.5723(1)	−0.9032(3)
$(B_3)_{T_c}$ (L/mol)^2	0.005914(2)	0.011901(6)	0.02112(2)	0.03473(4)	0.1090(3)	0.3012(8)
$(B_4)_{T_c}$ (L/mol)^3	$2.53(2) \times 10^{-4}$	$6.17(5) \times 10^{-4}$	0.00121(3)	0.002(1)(1)	0.0034	0.007(5)
$(B_5)_{T_c}$ (L/mol)^4	$3(4) \times 10^{-7}$	$-6(4) \times 10^{-6}$	$-1(5) \times 10^{-5}$	$-1(13) \times 10^{-5}$	−0.0023(3)	−0.017(2)
$(B_6)_{T_c}$ (L/mol)^5	$-1.2(2) \times 10^{-6}$	$-6(1) \times 10^{-6}$	$-1.7(6) \times 10^{-5}$			
$\rho_{c,sim}$ (g/ml)	0.206(3)	0.221(3)	0.231(6)	0.238(4)	0.239(2)	0.235(6)
$P_{c,sim}$ (MPa)	5.1(4)	4.4(1)	4.1(4)	3.7(1)	2.6(1)	2.3(2)
$P_{c,A5}$ (MPa)	5.2530(7)	4.618(1)	4.153(2)	3.78(3)	2.793(3)	2.135(4)
$P_{c,A6}$ (MPa)	5.281(1)	4.642(2)	4.176(5)			

Simulation values $T_{c,sim}$, $\rho_{c,sim}$ and $P_{c,sim}$ are taken from Martin and Siepmann [58]. Virial coefficients at $T_{c,sim}$ are obtained using an interpolation scheme[52] applied to the coefficients.[8] Approximant estimates $P_{c,A5}$ and $P_{c,A6}$ are computed using the nominal value of $\rho_{c,sim}$ and VEOS5 and 6 evaluated at $T_{c,sim}$ as inputs to (7) for each alkane. Numbers in parentheses specify the 68% uncertainty on the last digit, propagated from uncertainty in the virial coefficients (with the exception of the simulation values). P_c values computed using lower order approximants are shown in Figure 6.

are given in Table 3 along with $P_{c,A5}$, and $P_{c,A6}$. The deviation between the approximant predictions $P_{c,AJ}$ and nominal simulation values $P_{c,sim.}$ are shown in Figure 6, normalized by the uncertainty on $P_{c,sim}$ for each alkane (given in Table 3). As observed in the figure, all $P_{c,AJ}$ estimates converge to values that fall within the simulation error-bars, except those for propane and octane.

When applying the procedure above, we recommend choosing the available critical quantity of least precision (here, P_c) to adjust for critical scaling while using the nominal value of the quantity of highest precision (here, ρ_c) as an input to the approximant, as done above. Alternatively, one might try using the nominal simulation value of P_c as an input to the approximant and then adjust ρ_c within its error-bars until correct scaling is observed. This is equivalent to predicting ρ_c from the approximant using (7), as we did in the previous section. For TraPPE alkanes, we find that these estimates for ρ_c converge poorly with increasing order J to values that do not fall within the uncertainty of simulation data.

Finally, if T_c is given and at least $(B_2)_{T_c}$ is available, one may construct an approximant to predict both ρ_c and P_c using (4) in the following manner. Setting $a_J = a_{J-1} = 0$ in

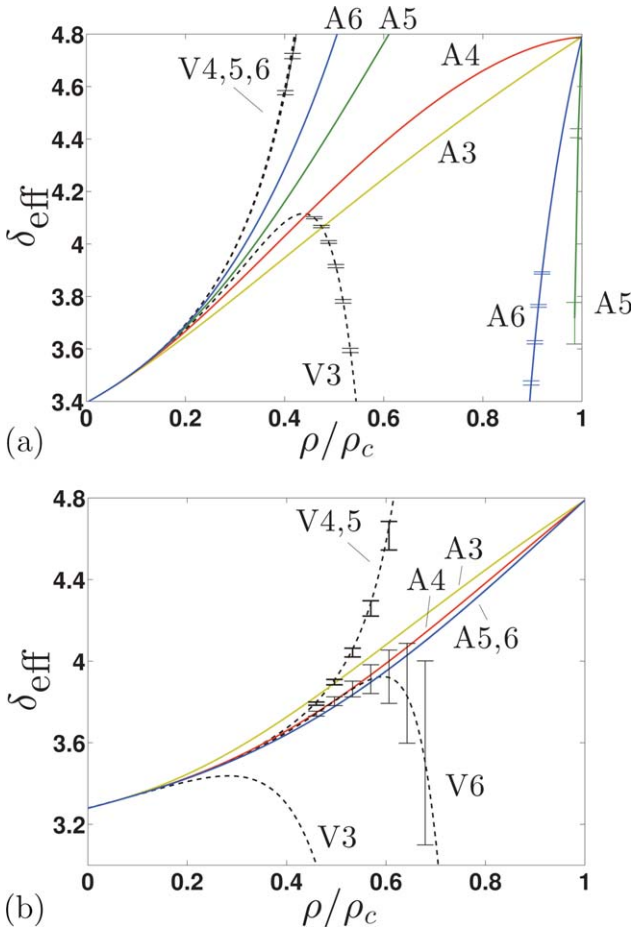

Figure 5. Approach to scaling along the TraPPE ethane critical isotherm as described by (5b) using $P(\rho)$ from the virial series (Eq. 1, - -, VEOSJ abbreviated as VJ) and the approximant (Eq. 4, —, AJ).

(a) using nominal P_c value from simulation[58] and (b) using the approximant prediction of P_c from (7) with $J = 6$. Note that curves A5 and A6 in (a) are discontinuous. Error-bars specify the 68% uncertainty, propagated from uncertainty in the virial coefficients. [Color figure can be viewed in the online issue, which is available at wileyonlinelibrary.com.]

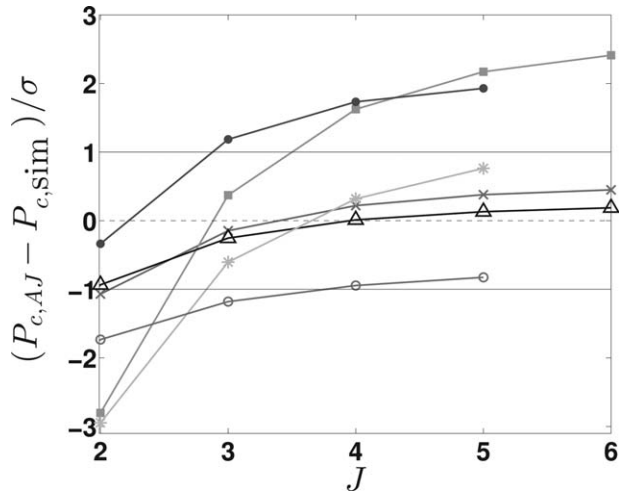

Figure 6. Deviation between $P_{c,AJ}$ from the approximant [using (7) and $\rho_{c,sim}$] and the nominal value of the critical pressure from simulation $P_{c,sim.}$, normalized by the uncertainty σ from simulation and plotted versus order J of the virial series used.

Molecular simulation values are taken from Ref. 58. The curves are shown for the following TraPPE alkanes: ethane (×), propane (■), butane (△), pentane (*), octane (•), dodecane (○). [Color figure can be viewed in the online issue, which is available at wileyonlinelibrary.com.]

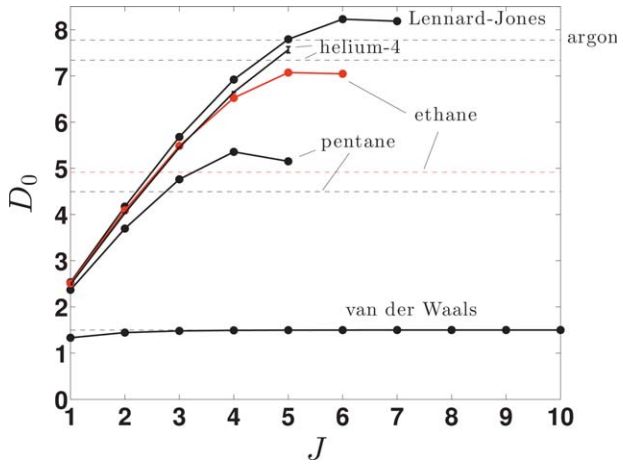

Figure 7. Critical amplitude D_0 for various fluids given by the approximant (4) using a J-term virial series; the alkane approximants use the "corrected" P_c values given in Table 3.

Literature values (- - -) for ethane, pentane, and argon are taken from the "restricted linear model" given in Behnejad et al.[16] (see references therein). For helium-4, we compare against the D_0 of the semiempirical model given in Bezverkhy et al.[56] For the van der Waals model, $D_0 = 3/2$. [Color figure can be viewed in the online issue, which is available at wileyonlinelibrary.com.]

(4b) leads to a system of 2 equations that can be solved for ρ_c and P_c. The $J-2$ coefficients of the approximant are then obtained using (4b). Note, that in such an approximant, we are decreasing the order of the polynomial $A(\rho)$ by 2 so that we may predict two quantities. Although we have examined this approach and obtained reasonable values, the low number of virial coefficients currently available do not allow us to report conclusive results on its efficacy here.

Critical amplitudes

Scaling laws, such as that expressed in (3), describe the critical behavior of all fluids in the same universality class, apart from two system-specific critical amplitudes needed to fully quantify the leading critical-point behavior. Given two amplitudes, all others can be evaluated from them via universal critical-amplitude ratios.[16] Given our restriction here to behavior on the critical isotherm, we can determine only one critical amplitude from our analysis, namely D_0 defined in (3). This quantity is difficult to determine from experiment or molecular simulation, but it is easily obtained from the approximant as the value of $A(\rho)/P_c$ at $\rho = \rho_c$. Of course, a complication arises from the weak confluent singularities in $A(\rho)$ at ρ_c, which restrict convergence, but in some cases it is possible to discern an estimated limit point. The behavior for the fluids examined above is presented in Figure 7, with comparison to the best available values from experiment (with argon standing in for the Lennard–Jones model). The figure indicates convergent behavior of D_0 with increasing order of the approximant. Convergence is (of course) perfect for the van der Waals equation of state, and it also appears to be good for the Lennard–Jones model and the alkanes. The value for He-4 is in good agreement with experiment, but it is unclear whether this value is converged. Differences of the alkane D_0 values with experiment could have a number of causes, including inaccuracies in the molecular model, or experimental error. Data from molecular simulations that use *ab initio* models would help to resolve this question, but it may be that new methods or new data analysis techniques are first needed before simulation can provide such information.

Comparison with a Crossover Model

Nonclassical scaling laws for critical phenomena apply only in a narrow range of conditions near the critical point, and considerable attention has been directed toward analysis and modeling of the crossover from classical analytical behavior to nonclassical behavior as the critical point is approached.[16,59–61] The starting point for these theories is the nonclassical asymptotic critical behavior, from which an attempt is made to build out into an extended region, moving away from the critical point. However, without additional information, crossover models cannot accurately capture behavior far from the critical region. Global crossover theories attempt to address this deficiency, providing the information needed to capture the correct behavior over large ranges of temperature and density, while also characterizing the behavior correctly in the critical region. Often this involves finding a method to connect the critical behavior to a traditional classical model such as a cubic equation of state.[35,62] The process typically requires the introduction of system-dependent parameters beyond those already present in the classical model. It is a challenge to develop such an approach that captures both the universal critical exponents and the amplitude ratios, while not introducing anomalous behavior in the classical region away from the critical point.

The virial-based approximant introduced in this work is too narrow in scope to be considered an archetypal crossover model, as it does not capture temperature dependence, nor does it extend beyond the critical density (because, as discussed above, our treatment does not remove all critical-point singularities). The lack of temperature dependence (as well as singularities at the binodal) precludes the extension of the approximant into the two-phase region (i.e., the approach does not characterize the shape of the coexistence curve). Furthermore, the approximant captures behavior appropriate to only one critical exponent, and it provides no description of the amplitude ratios. Still, it is worthwhile to examine how the critical isotherm approximant compares to a state-of-the-art crossover model within its range of application. This comparison is provided in Figures 8 and 3a for the Lennard–Jones fluid, using the crossover model described in Appendix C, which is based on the same seven-term virial series used to develop the approximant.

As shown in Figure 8a, the crossover model succeeds in going to zero pressure at $\rho = 0$, but the low-density virial series behavior input to the model is tainted by the crossover framework, and the equation of state does not even exhibit the correct ideal-gas limit (approaching instead $Z \equiv P/(\rho kT) \approx 1.1$; see inset). In contrast, the approximant adheres to the correct low-density behavior prescribed by the virial series, as designed. Additionally, the crossover model provides no correction to the critical density of the virial series, ρ_c^{cl}, thus both are ≈10% lower than the critical density of the approximant, as indicated by the vertical dashed line in Figure 8a.

The approach to the critical point is difficult to discern in Figure 8a, as all the curves become nearly flat (excluding the ideal gas law). This further complicates comparison of the approach to scaling between the approximant and the

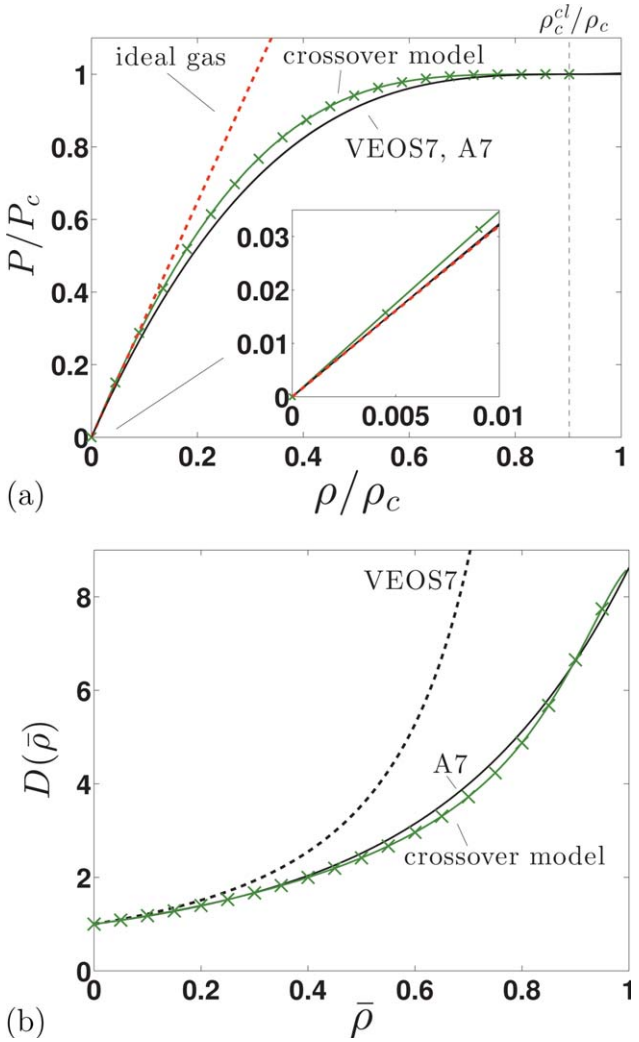

Figure 8. Critical isotherms for the Lennard–Jones fluid prescribed by the virial series (Eq. 1, VEOS7), the approximant (Eq. 4, A7), and a crossover model (Appendix C, –×–).

(a) Pressure versus "absolute" density, where ρ_c on the x-axis is $\rho_{c,A7}$ (i.e., the critical density of A7). Note that, on the scale of the inset, the ideal gas law, A7, and VEOS7 are indistinguishable from each other; the crossover model, however, has a visibly different slope. (b) $D(\bar{\rho})$ (Eq. 8) plotted on a "relative" scale, where $\bar{\rho}$ is $\rho/\rho_{c,A7}$ for the A7 curve and $\bar{\rho}$ is ρ/ρ_c^{cl} for VEOS7 and the crossover curve. ρ_c^{cl} is the critical density of both VEOS7 and the crossover model. [Color figure can be viewed in the online issue, which is available at wileyonlinelibrary.com.]

crossover model. To better discriminate between the crossover model, approximant, and virial series, it is useful to define the quantity

$$D(\rho)=\left[1-\frac{P(\rho)}{P_c}\right]\left(1-\frac{\rho}{\rho_c}\right)^{-\delta} \tag{8}$$

which is effectively the function describing all "corrections-to-scaling" along the critical isotherm, once the leading-order behavior has been removed. Note that $D(\rho)$ limits to the critical amplitude D_0 as $\rho \rightarrow \rho_c$ (see Eq. 3). For the approximant given by (4), $D(\rho)$ is simply $A(\rho)/P_c$. Since the approximant and the crossover models are based on different critical densities, to compare them we must evaluate (8) at the same reduced density (defined in terms of their respective ρ_c values). In Figure 8b, we compare $D(\rho)$ for each model on a relative scale (defined in the figure caption). When presented this way, we are able to see an agreement between the approximant and the crossover model in the approach to their respective critical regions; the figure also shows that they are largely in agreement over the entire density range. As in Figure 8b, the crossover model curve shown in Figure 3a is also plotted on a relative scale, using an x-axis of ρ/ρ_c^{cl}. Here, it is shown that the crossover model also attains the correct limit of $\delta_{eff} \rightarrow \delta$ as $\rho \rightarrow \rho_c$ and the approach to the critical point is close to that of the approximant.

Conclusions

Our aim going into this study was to leverage the universal critical behavior of fluids toward improving the convergence of the virial series on the critical isotherm, particularly with the goal of overcoming a systematic error that has consistently hampered its application for critical density estimation. The approximant developed here appears to have achieved this aim for systems where the virial series converges at densities approaching the critical region. In the process, we have found the approximant to be useful in ways we had not anticipated. In particular, it can be used to augment molecular simulation data to yield a critical pressure that is far more precise than possible from simulation data alone. Also, the approximant may be used as a probe of critical behavior, providing what may prove to be among the most effective ways to evaluate critical amplitudes. In its narrow scope of application (the critical isotherm for $\rho \leq \rho_c$), the relatively simple closed-form phenomenological treatment prescribed by the approximant describes the approach to the critical point in the same manner as a sophisticated crossover model built on renormalization-group theory. Yet, the ability of the approximant to offset the underestimation of ρ_c is not reproduced by the crossover model used here, which appears to be incapable of providing this correction (particularly given that it was not needed to adjust T_c, which appears to be the means by which it produces changes in ρ_c from the classical value).

The results presented here encourage development of a more comprehensive crossover model, one that captures the full spectrum of critical phenomena while fully adhering to the low-density behavior prescribed by the available virial coefficients. Perhaps this requirement can be met within such a framework using a higher-order Landau expansion[16] in the critical region. Complications are inevitable, however: mixed-field scaling should be used,[42] and the use of simpler formulations would require ad hoc adjustments to compensate for any lack of rigor in the selection of the scaling fields; also, it may be necessary to work with parametric variables,[16] to avoid anomalies in the global behavior. Extension to mixtures would likely work best using a representation of the mixture in terms of its species fugacity (or fugacity ratios), to avoid suppressing composition fluctuations on approach to the critical point; this of course compounds the challenges already facing pure-fluid applications.

Still, there is good reason to formulate models that are consistent with the virial series. One of the appealing features of the approximant proposed here is, that it is free of adjustable parameters (apart from the critical exponent δ, which is known independently). This is in fact a very

valuable element of virial-based approaches in general—virial coefficients for a given molecular model are determined rigorously, and can in principle incorporate effects of arbitrary complexity in a molecular model. With improvements to *ab initio* methods, molecular models, and computing hardware, we envision that in the long term, first-principles approaches to the prediction and analysis of critical phenomena will be feasible; more generally, they will be part of accurate first-principles models for gas-phase behavior covering a broad range of conditions. We see the developments presented in this work as important steps in that direction.

Acknowledgments

This work is supported by the U.S. National Science Foundation (NSF) (Grant No. CHE-1027963). N. S. Barlow is supported by an NSF award (Award No. CI-TraCS-1048579). Computational resources were provided by the University at Buffalo Center for Computational Research.

Literature Cited

1. Mason EA, Spurling TH. *The Virial Equation of State*. Pergammon Press: Oxford 1969.
2. McQuarrie DA. *Statistical Mechanics*. University Science Books, California, 2000.
3. Singh JK, Kofke DA. Mayer sampling: calculation of cluster integrals using free-energy perturbation methods. *Phys Rev Lett*. 2004; 92:220601.
4. Schultz AJ, Kofke DA. Sixth, seventh and eighth virial coefficients of the Lennard-Jones model. *Mol Phys*. 2009;107:2309–2318.
5. Schultz AJ, Barlow NS, Chaudhary V, Kofke DA. Mayer sampling Monte Carlo calculation of virial coefficients on graphics processors. *Mol Phys*. 2013;111:535–543.
6. Shaul KRS, Schultz AJ, Kofke DA. Path-integral Mayer-sampling calculations of the quantum Boltzmann contribution to virial coefficients of helium-4. *J Chem Phys*. 2012;137:184101.
7. Benjamin KM, Schultz AJ, Kofke DA. Fourth and fifth virial coefficients of polarizable water. *J Phys Chem B*. 2009;113:7810–7815.
8. Schultz AJ, Kofke DA. Virial coefficients of model alkanes. *J Chem Phys*. 2010;133:104101.
9. Barker JA, Leonard PJ, Pompe A. Fifth virial coefficients. *J Chem Phys*. 1966;44:4206.
10. MacDowell LG, Menduina C, Vega C, Miguel E. Critical properties of molecular fluids from the virial series. *J Chem Phys*. 2003;119: 11367.
11. MacDowell LG, Menduina C, Vega C, Miguel E. Third virial coefficients and critical properties of quadrupolar two center Lennard-Jones models. *Phys Chem Chem Phys*. 2003;5:2851.
12. Tester JW, Modell M. *Thermodynamics and Its Applications*. Upper Saddle River, NJ: Prentice Hall, 1997.
13. Levelt Sengers JMH, Greer WL, Sengers JV. Scaled equation of state parameters for gases in the critical region. *J Phys Chem Ref Data*. 1976;5:1.
14. Sengers JV, Levelt Sengers JMH. Critical phenomena in classical fluids. In: Croxton CA, editor. *Progress in Liquid Physics*, chapter 4. New York: Wiley, 1978: 103–174.
15. Levelt Sengers JMH, KamgarParsi B, Balfour FW, Sengers JV. Thermodynamic properties of steam in the critical region. *J Phys Chem Ref Data*. 1983;12:1.
16. Behnejad H, Sengers JV, Anisimov MA. Thermodynamic behaviour of fluids near critical points. In: Goodwin ARH, Sengers JV, Peters CJ., editors. *Applied Thermodynamics of Fluids*. Royal Society of Chemistry, Cambridge, UK, 2010.
17. Pelissetto A, Vicari E. Critical phenomena and renormalization-group theory. *Phys Rep*. 2002;368:549–727.
18. Chisholm JSR. Generalisations of Padé approximants. *Circuits Syst Signal Process*. 1982;1:279.
19. Maestre MÁG, Santos A, Robles M, De Haro ML. On the relation between virial coefficients and the close-packing of hard disks and hard spheres. *J Chem Phys*. 2011;134:084502.
20. Clisby N, McCoy BM. Ninth and tenth order virial coefficients for hard spheres in *D* dimensions. *J Stat Phys*. 2006;122:15–55.
21. Sanchez IC. Virial coefficients and close-packing of hard spheres and disks. *J Chem Phys*. 1994;101:7003–7006.
22. Ončák M, Malijevský A, Kolafa J, Labík S. On extrapolation of virial coefficients of hard spheres. *Condens Matter Phys*. 2012;15: 23004.
23. Bannerman MN, Lue L, Woodcock LV. Thermodynamic pressures for hard spheres and closed-virial equation-of-state. *J Chem Phys*. 2010;132:084507.
24. Baker GA Jr, Gammel JL. The Padé approximant. *J Math Anal Appl*. 1961;2:21–30.
25. Barlow NS, Schultz AJ, Weinstein SJ, Kofke DA. An asymptotically consistent approximant method with application to soft- and hard-sphere fluids. *J Chem Phys*. 2012;137:204102.
26. Baker GA Jr, Gilbert HE, Eve J, Rushbrook GS. High-temperature expansions for the spin-1/2 Heisenberg model. *Phys Rev*. 1967;164: 800–817.
27. Guttmann AJ. Asymptotic analysis of power series expansions. In: Domb C, Lebowitz J L., editors. *Phase Transitions and Critical Phenomena*, vol. 13, chapter 1, NY: Academic Press, 1989:1–234.
28. Guttmann AJ, Jensen I. Series analysis. In: Guttmann AJ., editor. *Polygons, Polyominoes, and Polycubes*, Springer, 2009.
29. Baker GA Jr. Application of the Padé approximant method to the investigation of some magnetic properties of the Ising model. *Phys Rev*. 1961;124:768–774.
30. Domb C. Critical properties of lattice models. In: *Critical Phenomenon: Proceedings of a Conference held in Washington, D. C., April 1965*, Collections of the University of Michigan Library, Published by Hewlett-Packard, Digitized by Google Books, 29–41.
31. Campostrini M, Pelissetto A, Rosi P, Vicari E. 25th-order high-temperature expansion results for three-dimensional Ising-like systems on the simple-cubic lattice. *Phys Rev E*. 2002;65:066127.
32. Thompson CJ. Mathematical Statistical Mechanics, chapter 6.5: Numerical Analysis of the Three-dimensional Ising Model. New Jersey: Princeton University Press, 1972.
33. Wheatley RJ. Calculation of high-order virial coefficients with applications to hard and soft spheres. *Phys Rev Lett*. 2013;110:200601.
34. Bondarev VN. The virial equation of fluid state and non-classical criticality. *Eur Phys J B*. 2011;84:121–129.
35. Wyczalkowska AK, Sengers JV, Anisimov MA. Critical fluctuations and the equation of state of van der Waals. *Phys A: Stat Mech Appl*. 2004;334:482–512.
36. Green MS, Cooper MJ, Levelt Sengers JMH. Extended thermodynamic scaling from a generalized parametric form. *Phys Rev Lett*. 1971;26:492–495.
37. Privman V, Hohenberg PC, Aharony A. Universal critical-point amplitude relations. In: Domb C, Lebowitz J L., editors. *Phase Transitions and Critical Phenomena*, vol. 14, chapter 1, NY: Academic Press, 1991: 1–134.
38. Markushevich AI. *Theory of functions of a complex variable*, chapter 1. Prentice-Hall, Englewood Cliffs, NJ, 1965.
39. Needham T. *Visual Complex Analysis*. New York: Oxford University Press, 2000.
40. Fisher ME, Orkoulas G. The Yang-Yang anomaly in fluid criticality: experiment and scaling theory. *Phys Rev Lett*. 2000;85:696.
41. Kim Y, Fisher M, Orkoulas G. Asymmetric fluid criticality. I. Scaling with pressure mixing. *Phys Rev E*. 2003;67:061506.
42. Anisimov M, Wang J. Nature of asymmetry in fluid criticality. *Phys Rev Lett*. 2006;97:025703.
43. Wegner FJ. Corrections to scaling laws. *Phys Rev B*. 1972;5:4529.
44. Anisimov MA. *Critical Phenomena in Liquids and Liquid Crystals*. Gordon and Breach Science Publishers, Singapore, 1991.
45. Vicentini-Missoni M, Levelt Sengers JMH, Green MS. Scaling analysis of thermodynamic properties in the critical region of fluids. *J Res Natl Bur Stand Sect A: Phys Chem*. 1969;73A:563–583.
46. Centek W, Patkowski K, Szalewicz K. Full-configuration-interaction calculation of three-body nonadditive contribution to helium interaction potential. *J Chem Phys*. 2009;131:064105.
47. Przybytek M, Centek W, Komasa J, Lach G, Jeziorski B, Szalewicz K. Relativistic and quantum electrodynamics effects in the helium pair potential. *Phys Rev Lett*. 2010;104:183003.
48. Paricaud P, Předota M, Chialvo AA, Cummings PT. From dimer to condensed phases at extreme conditions: accurate predictions of the properties of water by a Gaussian charge polarizable model. *J Chem Phys*. 2005;122:244511.
49. Pérez-Pellitero J, Ungerer P, Orkoulas G, Mackie A. Critical point estimation of the Lennard-Jones pure fluid and binary mixtures. *J Chem Phys*. 2006;125:054515.

50. Potoff JJ, Panagiotopoulos AZ. Critical point and phase behavior of the pure fluid and a Lennard-Jones mixture. *J Chem Phys*. 1998;109:10914.
51. Kukarin VF, Martynets VG, Matizen ÉV, Sartakov AG. Approximation of $P-\rho-T$ data near the critical point for He^4 with a new equation of state. *Low Temp Phys*. 1981;7:725–728.
52. Schultz AJ, Kofke DA. Interpolation of virial coefficients. *Mol Phys*. 2009;107:1431–1436.
53. Kolafa J, Nezbeda I. The Lennard-Jones fluid: an accurate analytic and theoretically-based equation of state. *Fluid Phase Equilib*. 1994; 100:1–34.
54. Johnson JK, Zollweg JA, Gubbins KE. The Lennard-Jones equation of state revisited. *Mol Phys*. 1993;78:591–618.
55. Lemmon EW, Linden MO, Friend DG. Thermophysical properties of fluid systems. In: Linstrom PJ, Mallard WG, editors. *NIST Chemistry WebBook, NIST Standard Reference Database Number 69*, National Institute of Standards and Technology, Maryland, US, Accessed on September 11, 2013.
56. Bezverkhy PP, Martynets VG, Matizen EV. Equation of state for ^{4}He, including a regular and a scalar part. *Low Temp Phys*. 2009;35:741–747.
57. Kim HM, Schultz AJ, Kofke DA. Virial equation of state of water based on Wertheim's association theory. *J Phys Chem B*. 2012;116: 14078–14088.
58. Martin MG, Siepmann JI. Transferable potentials for phase equilibria. 1. United-atom description of *n*-alkanes. *J Phys Chem B*. 1998; 102:2569.
59. Tang S, Sengers JV, Chen ZY. Nonasymptotic critical thermodynamical behavior of fluids. *Phys A: Stat Mech Appl*. 1991;179:344–377.
60. Anisimov MA, Kiselev SB, Sengers JV, Tang S. Crossover Approach to global critical phenomena in fluids. *Phys A: Stat Mech Appl*. 1992;188:487–525.
61. Anisimov MA, Sengers JV. Critical region. In: Sengers JV, Kayser R F, Peters C J, White H J., editors. *Equations of State for Fluids and Fluid Mixtures*, Elsevier, Amsterdam, The Netherlands, 2000: 381–434.
62. Kiselev SB. Cubic crossover equation of state. *Fluid Phase Equilib*. 1998;147:7–23.
63. Chen ZY, Albright PC, Sengers JV. Crossover from singular critical to regular classical thermodynamic behavior of fluids. *Phys Rev A*. 1990;41:3161–3177.
64. Chen ZY, Abbaci A, Tang S, Sengers JV. Global thermodynamic behavior of fluids in the critical region. *Phys Rev A*. 1990;42:4470–4484.

Appendix A: Ideal-Gas/Critical-Scaling Approximant

The $J=1$ critical approximant (A1) is given by

$$\left(\frac{P}{P_c}\right)_{T_c}=1-\left[1-\left(\frac{1}{Z_c}-\delta\right)\frac{\rho}{\rho_c}\right]\left(1-\frac{\rho}{\rho_c}\right)^{\delta} \tag{9}$$

for any fluid, since $B_1=1$ for any fluid (ideal gas limit as $\rho\to 0$). Additionally, the value of $1/Z_c=\rho_c kT_c/P_c$ is approximately the same across groups of fluids, allowing us to collapse A1 and critical isotherm data from experiments onto only a few curves for most common fluids. We have done this for several fluids listed in the NIST webbook.[55] We present results for three of them in Figure 9, which shows a comparison of the critical isotherms for water ($1/Z_c=4.3592$), argon ($1/Z_c=3.4542$), and hydrogen ($1/Z_c=3.2971$). For all fluids shown, the critical approximant A1 is an improvement over the ideal gas law when representing data interpolated from experiments. As demonstrated in the main text, the accuracy of the approximant is improved by including additional virial coefficients.

Appendix B: Convergence of P_c to a Branch-Point in ρ_c

Consider a model fluid expressed in dimensionless quantities where $\rho_c=1$, $P_c=1$, and $kT_c=10/3$, such that it falls on the near-universal curve of Figure 9. Substituting these values into (9) (for the region $\rho\le\rho_c$) gives an expression for the fluid's critical isotherm that satisfies both the ideal-gas law and critical scaling: $P=1-[1-(10/3-\delta)\ \ \rho](1-\rho)^{\delta}$. In what follows, we treat this equation as exact, and consider how well a virial series for this model would predict the respective critical properties. Taking $\delta=4.789$, the J-term expansion about $\rho=0$ of this equation provides us with a virial series of a nonclassical model fluid to any order J for a fixed value of T_c. Note that in practice, predictions of T_c fluctuate with the order of truncation J. Applying definitions (2) to determine the critical point of the model fluid described above leads to the predictions in Table 4. Since $\delta=4.789$ prescribes a slowly varying pressure region surrounding the critical point, convergence to the correct P_c value is possible at a faster rate than that of ρ_c, which is approached slowly from below. This is expected, as ρ_c is the radius of convergence of the virial series here, and demonstrates why predictions of ρ_c from the virial series are typically found to be too low in general while those of P_c and T_c are essentially correct.

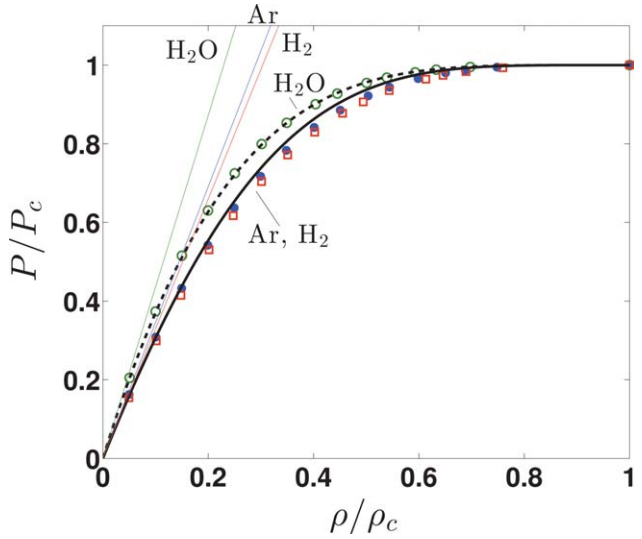

Figure 9. Critical isotherms as prescribed by the A1 approximant (9) (- - H_2O, — Ar and H_2), interpolation through data from experiments[55] (○ H_2O, • Ar, and □ H_2), and the ideal gas law (thin diagonal lines).

[Color figure can be viewed in the online issue, which is available at wileyonlinelibrary.com.]

Table 4. Points Where $\frac{\partial P}{\partial \rho}=0$ in Model Fluid

J	ρ_c	P_c	$\frac{\partial^2 P}{\partial \rho^2}$
10	0.9078	0.99988424	−0.0710
20	0.9587	0.99999695	−0.0076
30	0.9733	0.99999960	−0.0023
40	0.9803	0.99999990	−0.0010
50	0.9844	0.99999997	−0.0005

The approach to $\frac{\partial^2 P}{\partial \rho^2}=0$ is shown in the last column.

Appendix C: Crossover Model

Here we describe the global equation of state used as the crossover model for the comparison presented in Figures 8 and 3a. The only novel feature of this treatment is the use of the virial series as the classical model. Hence, we do not attempt to review the ideas underlying this development, but focus only on enumerating the steps taken to compute the pressure according to the crossover model. To conserve space, the description here is specific to a fluid on its critical isotherm, and omits any elements needed to capture the general temperature dependence.

Further, we do not incorporate details needed to distinguish the critical temperature T_c of the classical virial series model from the true T_c obtained using any nonclassical treatment of the critical point, because we know that these are essentially the same for the Lennard–Jones model used for this demonstration (cf. Table 2). For additional details, one can consult the literature;[16,59,63,64] our development follows closely to that given in Wyczalkowska et al.[35]

We start with quantities defined for the virial series classical model

$$\bar{\rho}=\frac{\rho}{\rho_c^{cl}} \qquad \bar{P}=\frac{P}{P_c} \qquad \bar{\mu}=\mu\frac{\rho_c^{cl}}{P_c}$$

$$\bar{\chi}=\chi\frac{P_c}{\left(\rho_c^{cl}\right)^2} \qquad \bar{A}=\frac{\rho A}{P_c} \qquad \Delta\bar{\rho}=\bar{\rho}-1$$

where μ is the chemical potential, $\chi=(\partial\rho/\partial\mu)_T$ is the isothermal susceptibility, and A is the molar Helmholtz free energy. The superscript "cl" on ρ_c indicates it is the value obtained from the classical virial series; we omit this designation on P_c because it, like T_c, is not substantially different from the true P_c for the Lennard–Jones model.

In terms of these variables, the virial series, (1), is

$$\bar{P}(\bar{\rho})=\frac{1}{Z_c^{cl}}\sum_{j=1}^{J}\bar{B}_j\bar{\rho}^j, \quad \bar{B}_j\equiv B_j\left(\rho_c^{cl}\right)^{j-1}$$

where $Z_c^{cl}=P_c/\rho_c^{cl}kT_c$. We use $J=7$ in this demonstration. Then

$$\bar{\mu}=\bar{\mu}_0+\int(\Delta\bar{\rho}+1)^{-1}(\partial\bar{P}(\Delta\bar{\rho}+1)/\partial\Delta\bar{\rho})d\Delta\bar{\rho}$$

$$\bar{A}=\bar{\rho}\bar{\mu}-\bar{P}$$

$$\bar{\chi}^{-1}=(\partial^2\bar{A}/\partial\bar{\rho}^2)$$

where $\bar{\mu}_0$ is a constant of integration, defined such that $\bar{\mu}-\bar{\mu}_0=0$ for $\Delta\bar{\rho}=0$. The Helmholtz free energy is separated into a background part $\bar{A}_0$ and a part $\Delta\bar{A}$ that is impacted by critical fluctuations in the nonclassical treatment, thus

$$\bar{A}=\Delta\bar{A}+\bar{\rho}\bar{\mu}_0+\bar{A}_0$$

$\bar{A}_0$ is defined such that $\Delta\bar{A}=0$ at $\Delta\bar{\rho}=0$, and it is equal to -1.

Now we can introduce the terms needed for the crossover treatment. A tilde is used instead of the overbar to indicate quantities given by the nonclassical model. These are made dimensionless just as the quantities with the overbar, but using the true ρ_c instead of ρ_c^{cl}, and they are formulated to have a nonclassical density dependence near the critical point. First, we have the nonclassical free energy, which for the crossover model is given by the classical free energy, but evaluated at a scaled density (written here for $T=T_c$): $\Delta\tilde{A}(\tilde{\rho})=\Delta\bar{\bar{A}}(\Delta\tilde{\rho}_\times)$, with $\Delta\tilde{\rho}_\times=\mathscr{R}(Y)\Delta\tilde{\rho}$, $\mathscr{R}(Y)=Y^{\nu(1-2\eta)/4\Delta_s}$; $Y(\Delta\tilde{\rho})$ is a crossover function defined below. The exponents in the definition of $\mathscr{R}$ are: $\nu=0.6301$, $\eta=0.0364$ (taken from Pelissetto and Vicari,[17] such that $\delta=4.789$), and $\Delta_s=0.52$. The free energy $\Delta\bar{\bar{A}}(\Delta\tilde{\rho}_\times)$ is almost the same as developed above, but substituting a slightly different scaling for the leading asymmetric contribution, so it is given by $\Delta\bar{\bar{A}}(\Delta\tilde{\rho}_\times)=\Delta\bar{A}(\Delta\tilde{\rho}_\times)+\Delta\bar{A}_5\Delta\tilde{\rho}_\times^5\left(\mathscr{V}\mathscr{U}^{-1/4}-1\right)$, where $\mathscr{U}(Y)=Y^{\nu/\Delta_s}$, $\mathscr{V}(Y)=Y^{(\Delta_a-1/2)/\Delta_s}$, $\Delta_a=1.32$, and the constant $\Delta\bar{A}_5$ is the fifth-order term in the expansion of $\Delta\bar{A}(\Delta\bar{\rho})$ about $\Delta\bar{\rho}=0$.

A quantity κ is introduced as: $\kappa^2(Y;\Delta\tilde{\rho})=c_\rho^{-2}\bar{\bar{\chi}}^{-1}(\Delta\tilde{\rho}_\times)[\mathscr{U}(Y)]^{1/2}$. Here, c_ρ is a constant given by $c_\rho^{-2}=(u^*\bar{u}\Lambda/u_0)^{1/2}$, where $u^*=0.472$, while $\bar{u}$ and Λ are physically meaningful but adjustable crossover-model parameters. As with $\bar{\bar{A}}$, the isothermal susceptibility $\bar{\bar{\chi}}^{-1}(\Delta\tilde{\rho}_\times)$ substitutes the leading asymmetric contribution: $\bar{\bar{\chi}}^{-1}(\Delta\tilde{\rho}_\times)=\bar{\chi}^{-1}(\Delta\tilde{\rho}_\times)+\bar{\chi}_3^{-1}\Delta\tilde{\rho}_\times^3(\mathscr{V}^{3/5}\mathscr{U}^{-3/20}-1)$, where the constant $\bar{\chi}_3^{-1}$ is the third-order term in the expansion of $\bar{\chi}^{-1}(\Delta\bar{\rho})$ about $\Delta\bar{\rho}=0$. We can now define the crossover function $Y(\Delta\tilde{\rho})$ as the solution to

$$1-(1-\bar{u})Y=\bar{u}Y^{\nu/\Delta_s}\left[1-\Lambda^2/\kappa^2(Y;\Delta\tilde{\rho})\right]^{1/2}$$

which is solved numerically for Y for a given $\Delta\tilde{\rho}$.

Finally, the pressure is obtained according to

$$\tilde{P}(\tilde{\rho})=\tilde{\rho}(\partial\Delta\tilde{A}/\partial\Delta\tilde{\rho})-\Delta\tilde{A}(\Delta\tilde{\rho})-\bar{A}_0$$

The derivative in this expression is evaluated via the chain rule applied to $\bar{\bar{A}}(\Delta\tilde{\rho}_\times)$. The necessary derivative $Y'\equiv\partial Y/\partial\Delta\tilde{\rho}$ is evaluated via implicit differentiation of the equation for Y, which allows for the explicit solution of Y' in terms of Y and $\Delta\tilde{\rho}$.

For the adjustable parameters, Λ is expected to be of order unity[35] for this class of systems, so we use $\Lambda=1$. We set $\bar{u}=0.237906$ by forcing the critical amplitude D_0 to exactly match that of the approximant used in the main text (Fig. 8b, at $\bar{\rho}=1$). It is pleasing to find that this choice is consistent with the recommended value of $\bar{u}=0.24$ for systems having a Lennard–Jones type attraction.[35]

Manuscript received Jan. 31, 2014; and revision received June 3, 2014.